

Temperature, magnetic field, and pressure dependence of the crystal and magnetic structures of the magnetocaloric compound $\text{Mn}_{1.1}\text{Fe}_{0.9}(\text{P}_{0.8}\text{Ge}_{0.2})$

D. M. Liu¹, Q. Huang², M. Yue¹, J. W. Lynn^{2*}, L. J. Liu¹, Y. Chen^{2,3}, Z. H. Wu⁴, J. X. Zhang¹

¹*Key Laboratory of Advanced Functional Materials Ministry of Education, Beijing University of Technology, 100 Pingleyuan, Chaoyang District, Beijing 100022, China*

²*NIST Center for Neutron Research, National Institute of Standards and Technology, Gaithersburg, Maryland 20899*

³*Department of Materials Science and Engineering, University of Maryland, College Park, Maryland 20742*

⁴*Neutron Scattering Laboratory, China Institute of Atomic Energy, P.O. Box 275(30), Beijing 102413, China*

ABSTRACT

Neutron powder diffraction studies of the temperature, magnetic field, and pressure dependence of the crystal and magnetic structures of $\text{Mn}_{1.1}\text{Fe}_{0.9}(\text{P}_{0.8}\text{Ge}_{0.2})$ demonstrate that there is a single, combined magnetic and structural, first-order transition from the paramagnetic (PM) to ferromagnetic (FM) phase ($T_c \approx 255$ K for this composition). The structural part of the transition is associated with an expansion of the hexagonal unit cell in the direction of the a - and b -axes and a contraction of the c -axis as the FM phase is formed, which originates from an increase in the intra-layer metal-metal bond distance. Our measurements confirm that the application of pressure has an adverse effect on the formation of the FM phase since pressure opposes the expansion of the lattice and hence decreases T_c . The application of a magnetic field, on the other hand, has the expected effect of enhancing the FM phase and increasing T_c . We find that the coexistence of the PM and FM phases for a range of temperature/field/pressure values is due to compositional differences in different parts of the sample, suggesting that the properties of this compound can be optimized by preparing samples of homogeneous composition.

PACS: 75.30.Sg; 75.30.Kz; 64.70.K-; 61.05.fm

I. INTRODUCTION

Magnetic refrigeration based on the magnetocaloric effect (MCE) has attracted recent interest as a potential replacement for the classical vapor compression systems in use today, because it offers potential energy savings, it doesn't use gases harmful to the atmosphere, the system is more compact because the working material is a solid, and its operation should be significantly quieter.¹ In general one wants as large an MCE as possible for the working material, and one way to increase this is to have a system that has a combined magnetic and structural transition, thereby circumventing the limitation imposed by relying only on the magnetic entropy of the system for the thermodynamic cycle. This has led to the *giant* magneto-caloric effect found in $\text{MnAs}_{1-x}\text{Sb}_x$ ^{ref. 2} and $\text{Gd}_5\text{Si}_2\text{Ge}_2$ ^{ref. 3}. The closely related hexagonal $\text{MnFeP}_{1-x}\text{As}_x$ compound was found to have a first-order transition from a paramagnetic to a ferromagnetic phase which exhibits a huge MCE.⁴ However, the high cost of Gd and the toxicity of As makes it unlikely that these compounds will have widespread commercial applications. Recently, it was found that by replacing As with Ge and Si, a large MCE can be achieved near room temperature in a magnetic field ranging from 0 to 5 T⁵⁻¹¹. In particular, we tuned the compound $\text{Mn}_{1.1}\text{Fe}_{0.9}\text{P}_{0.8}\text{Ge}_{0.2}$ to have a value of MCE of 75 J/kg-K, almost double that of the previous reports.¹² In this study it was found that the compound undergoes a first-order structural and magnetic phase transition from a paramagnetic (PM) to a ferromagnetic (FM) phase at about 255 K. The two phases were shown to have distinct crystal structures with the same the Fe_2P -type hexagonal symmetry, with the magnetic entropy varying directly with the fraction of each phase as a function of magnetic field or temperature. Thus the

MCE was completely governed by the transformation from one crystal and magnetic phase to the other.

In the present study we have used neutron diffraction to explore the crystal and magnetic structural properties as a function of temperature, pressure, and magnetic field, focusing on the properties in the region of the PM-FM transition where the MCE properties are of most interest. The purpose is to reveal the relationships between the crystal structure and magnetic properties in this regime, to identify the factors that control the presence of the two phases in the sample.

II. EXPERIMENTAL DETAILS

High resolution powder diffraction data were collected at the NCNR on the BT-1 high-resolution neutron powder diffractometer, using monochromatic neutrons of wavelength 1.5403 Å produced by a Cu(311) monochromator. Söller collimations before and after the monochromator and after the sample were 15', 20', and 7' full-width-at-half-maximum

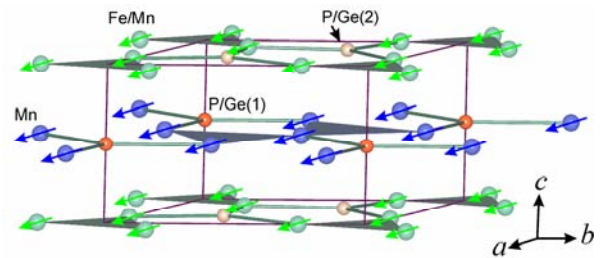


Fig. 1. (color online) Atomic positions and magnetic structure of the ferromagnetic phase. Both the Fe and Mn moments are ordered ferromagnetically, with the moments lying in the a - b plane. A magnetic structure with $P11m'$ symmetry (moments along the a -axis) was used in the refinements. The refined ordered moments at 10 K are 2.9(1) μ_B and 1.7(1) μ_B for the Mn (pyramidal) and the Fe/Mn (tetrahedral) sites, respectively.

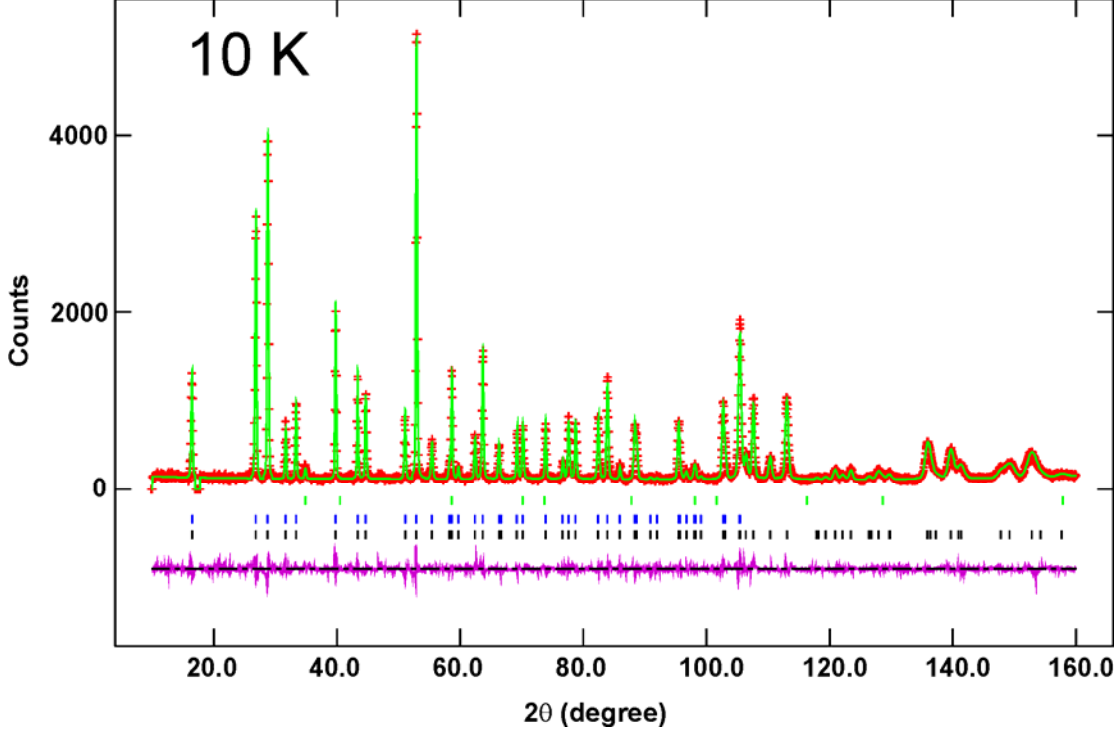


Fig. 2. (color online) Observed (crosses) and calculated (continuous lines) intensities for data collected at 10 K, where only the FM phase is present. Differences are shown in the low part of the plots. Vertical lines indicate the angular positions of the diffraction lines for the nuclear (bottom), magnetic (middle), and impurity (top) structures, respectively. The impurity peaks (due to MnO) were taken into account in the refinements.

(FWHM), respectively. Data were collected in the 2θ range of 3° to 168° with a step size of 0.05° for various temperatures from 300 K to 5 K. Magnetic field measurements were carried out with a vertical field 7 T superconducting magnet, and the structural refinements were performed in the same manner as previously.¹² The sample was the identical one that was used in the earlier study.

Detailed temperature, magnetic field, and pressure-dependent measurements were carried out on the high-intensity BT7 and BT9 triple axis spectrometers. For the pressure measurements, a stainless-steel cell was employed with a maximum pressure of 1.0 GPa, with helium gas as the pressure medium. On each instrument a pyrolytic graphite (PG) (002) monochromator was employed to

provide neutrons of wavelength 2.36 \AA , and a PG filter was used to suppress higher-order wavelength contaminations. Coarse collimations of $60'$, $50'$, and $50'$ full-width-at-half-maximum (FWHM) on BT7 and $40'$, $48'$, and $40'$ FWHM on BT9 were employed to maximize the intensity. No energy analyzer was used in these measurements.

III. RESULTS

$\text{Mn}_{1.1}\text{Fe}_{0.9}\text{P}_{0.8}\text{Ge}_{0.2}$ has the Fe_2P -type hexagonal structure, space group $P\bar{6}2m$, and the symmetry of the magnetic structure is $P11m'$. As shown in Fig. 1, the Mn atoms are coplanar with the P/Ge(1) atoms, and the Fe/Mn atoms are coplanar with P/Ge(2). The intra-plane transition metals form a triangular configuration. The Mn atoms are surrounded

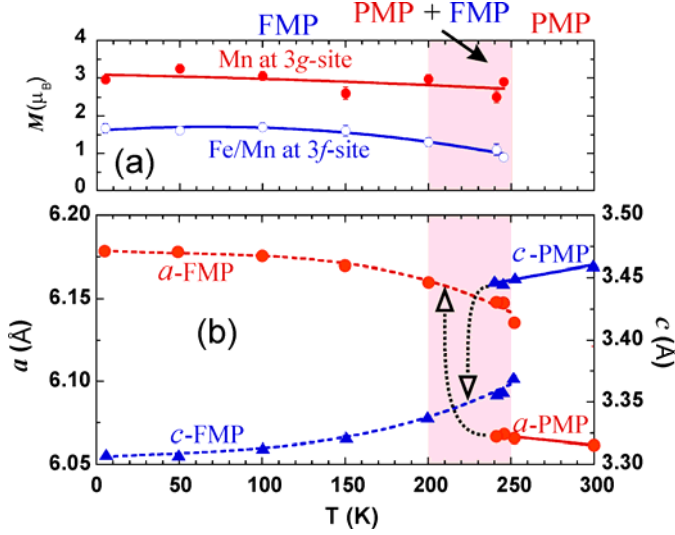


Fig. 3. (color online) Lattice parameters of the PMP and FMP and magnetic moments of Mn and Fe/Mn atoms as a function of temperature. The c -axis lattice parameter sharply decreases in going from the PMP to FMP, while the a -axis lattice parameter increases. The magnetic moment of the Mn does not significantly change over the entire range of temperatures, while the moment on the Fe/Mn site exhibits a very modest decrease at elevated temperatures.

by four P/Ge(2) atoms located on the layers above and below and by one apical P/Ge(1) atom on the same layer, forming a pyramid. The Fe/Mn site is coordinated by two P/Ge(2) atoms located on the same layer and two P/Ge(1) atoms in the layers above and below, forming a tetrahedron.

The data and combined magnetic and structural refinement fit at 10 K, with ambient magnetic field and pressure, are shown in Fig. 2. The agreement between observed and calculated intensities, shown in this figure as an example, is excellent. The quantitative results of the refinements are given in Table 1, where they are compared with the results reported in Ref. [12] for a temperature of 295 K. The relevant bond distances are provided in Table 2.

The temperature variations of the lattice parameters and of the Fe and Mn magnetic

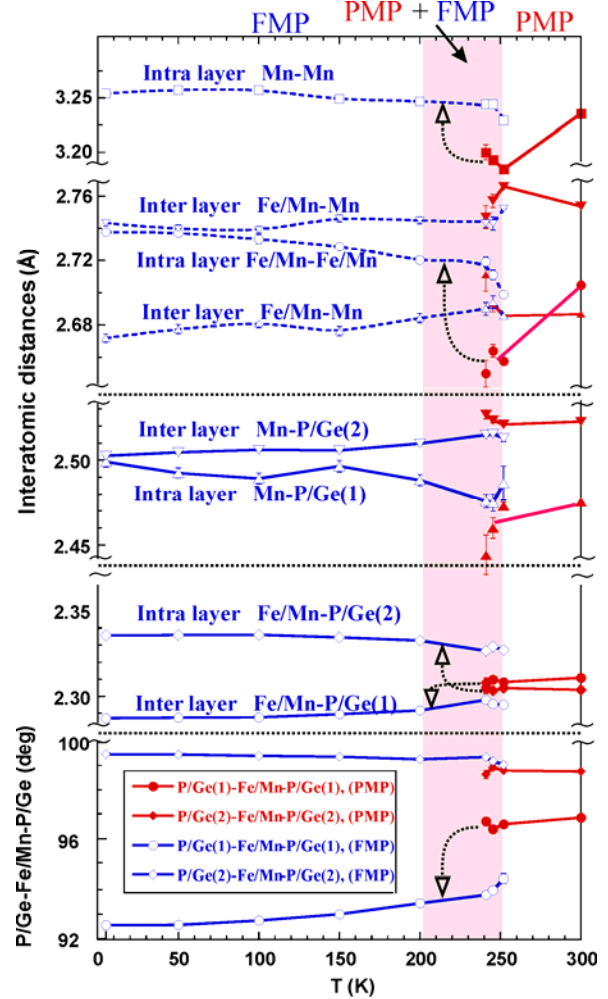


Fig. 4. (color online) Variation of the metal-metal bond distances as function of temperature. The changes occurring at the transition are indicated by the arrows.

moments for the paramagnetic phase (PMP) and ferromagnetic phase (FMP) are shown in Fig. 3, and the temperature dependence of the relevant metal-metal bond distances are shown in Fig. 4. We see that the a -axis lattice parameter increases and the c -axis lattice parameter decreases abruptly at the transition, as previously indicated. From the figures it is readily discerned that, aside from the sharp changes that occur at the phase transition, there is little variation with temperature. It is interesting to note that, while the intra-layer metal-metal bond distances show a

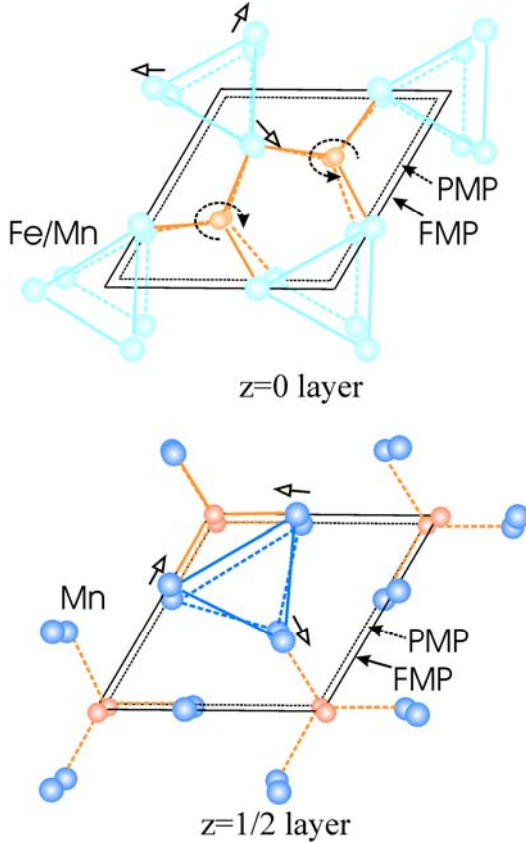


Fig. 5. (color online) Projections along the c -axis of the atomic arrangement in the $z=0$ - and $z=1/2$ -layers of the structure. The atomic shifts and the rotations about the P/Ge atoms taking place at the transition are indicated by the arrows. The outlines of the unit cell, and the bonds between the atoms, are shown by continuous and broken lines for the FMP and PMP, respectively.

significantly large increase in going from the PM to FM phase, the inter-layer distances either remain approximately constant or decrease slightly, in spite of the large decrease of the c -axis lattice parameter. The data in Fig. 3 and 4 also show that the shortening of the c -axis is mainly due to a decrease of the P/Ge(1)-Mn-P/Ge(1) angle (about 4%).

Fig. 5 shows the relative atomic positions in the a - b plane in the PM and FM phases. The atomic shifts between the two

phases are indicated by the arrows, and their effect on the bond distances is clearly visible. In particular, on the $z=0$ layer, the Fe/Mn-Fe/Mn distances sharply increase, as do the Fe/Mn-P/Ge(2) distances. These atomic readjustments are facilitated by the indicated rotations taking place about the P/Ge(2) atoms. On the $z=1/2$ layer, the same behavior occurs for the Mn-Mn distances, with only a slight variation of the Mn-P/Ge(1) separations.

A close look at the atomic arrangement illustrated in Fig 5 reveals that the bond distances most affected by the phase transformation are the metal-metal distances in both layers, resulting in an expansion of the triangular disposition of the atoms. Since the metal atoms are the ones that are involved in the magnetic coupling, it is clear that the structural and magnetic transitions are intimately related to one another, and therefore any factor that affects these interatomic distances will have an effect, in one direction or the other, on the transition temperature. In particular, from these results we may conclude that the ferromagnetic state is facilitated (and the value of T_c increased) by those factors that tend to cause an expansion in the a - and b -directions of the cell, and this, in turn, underlines the importance of the type of doping used in an effort to improve the properties of the system. The crystallographic data reveal that changes in the value of T_c can be obtained not only by external factors such as pressure or magnetic field, but also by changes in the internal unit cell provided by altering the composition of the compound. Examples of such procedures are rather common, for example, in superconducting materials¹⁴. Clearly, the substitution of P with larger atoms like Si or Ge⁸ would be advantageous, but there are limitations that we have to consider. For example, replacing P with Ge, which has a much larger covalent radii (1.06 and 1.22 Å, respectively), creates stresses in the structure,

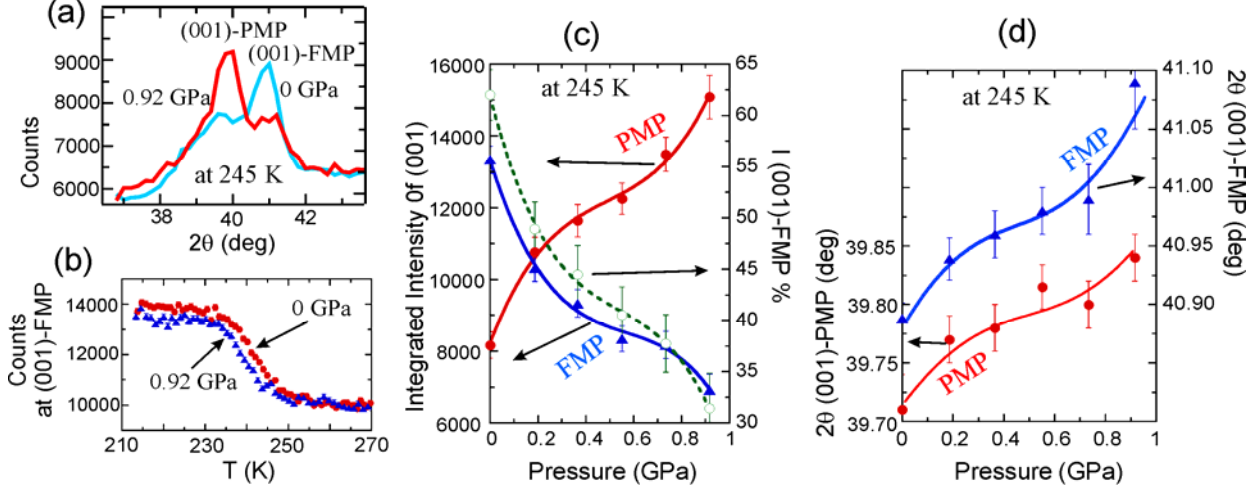


Fig. 6. (color online) Pressure dependence of the scattering measured at 245 K on BT9. (a) (001) peak profiles of the PMP and FMP at 0 (blue line) and 0.92 (red line) GPa. At ambient pressure the intensity of the FM peak is higher than that at 0.92 GPa, and the contrary is observed for the intensity of the PM peak. (b) Intensity of the (001) FM peak as function of temperature for ambient pressure and 0.92 GPa, showing that the transition temperature decreases when pressure is applied. (c) Integrated intensities for the PM and FM reflections as a function of pressure, showing that the intensity of (001)-PM peak increases and that of the (001)-FM peak decreases. The green broken line shows the relative intensities of the two peaks. (d) Angular position of the two peaks as a function of pressure. These data show that the lattice parameters of both phases decrease as the pressure increases, as expected.

and these may have an adverse effect on the value of T_c and on the range of coexistence of the two phases.

The above analysis also explains the effect of pressure on T_c . The application of pressure should inhibit the formation of the FM phase (and decrease T_c) because it opposes the expansion of the triangular arrangement of the metal atoms. This is, in fact, what we observe, as shown in Table 3 and in Fig. 6.

From the Table we find that, at 239 K and ambient pressure, the phase fractions of the PM and FM phases are 19.8 and 80.2%, respectively. At a pressure of 0.92 GPa, however, the phase fraction of FM phase is reduced to 73.5% and that of the PM phase increased to 26.5%. Consistent with these results, Fig. 6 shows the variations of the intensity of the 001 reflections of the PM and FM phases at 245 K, and 0 and 0.92 GPa pressure, as function of the scattering angle

(Fig. 6a) and as function of temperature (Fig. 6b), where the transition temperature decreases by ~ 3 K under 0.92 GPa. The effect of pressure is particularly evident in Fig. 6c, where the integrated intensity of the PM (001) reflection increases, and that of the FM (001) reflection decreases, as the pressure increases. Moreover, the pressure dependence of the phase transition (Fig. 6c) and (001) peak positions (Fig. 6d) are smooth but nonlinear. The increase in the (001)-PMP intensity and the decrease in the c -axis (increasing in 2θ of the (001)-PMP) indicate that the spin ordering is highly correlated to the lattice constants, *i.e.* pressure decreases the metal-metal distances and, therefore, inhibits the formation of the FMP.

Fig. 7 shows the effect of an applied magnetic field on the PM-FM transition. The variation of the FMP fraction and the changes of the unit cell volumes of the two phases as a function of the strength of the magnetic field

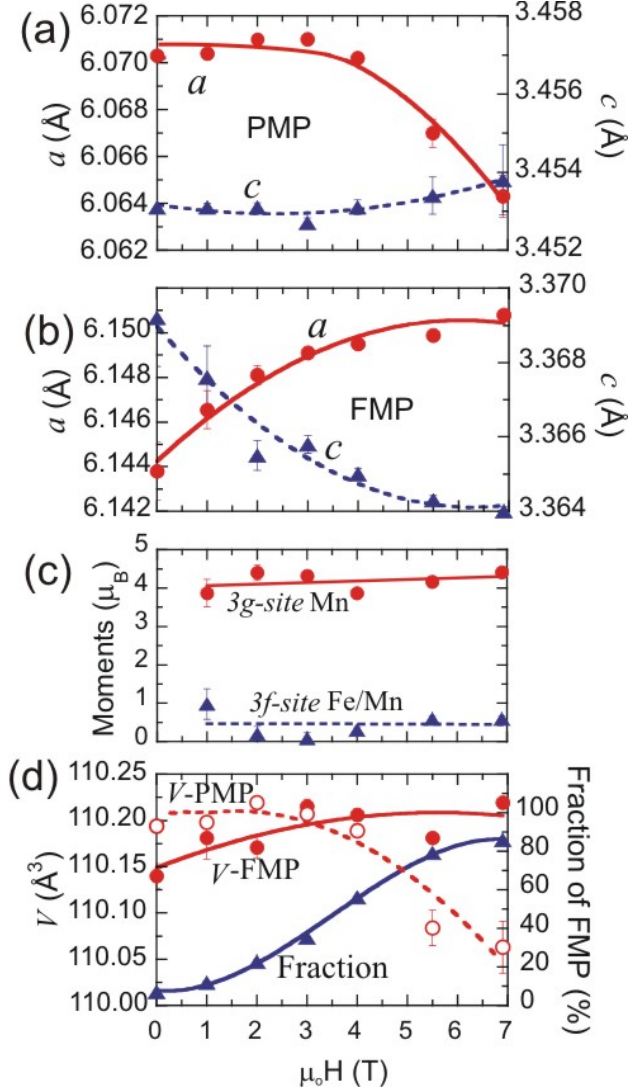


Fig. 7. (color online) Variation of the lattice parameters (Figs 7a and 7b) and of the unit cell volume (Fig. 7d) as a function of applied magnetic field for (a) the PMP and (b) the FMP. (c) The ordered magnetic moments for the Mn and Mn/Fe sites do not vary with field. (d) Fraction of the sample that is ferromagnetic vs. applied magnetic field, and volume of the unit cell for the PMP and FMP.

are shown in Fig. 7d, for a temperature of 255 K. As expected, the FMP fraction increases with the applied field, which is consistent with the fact that the magnetic field induces the ordering of the spins and therefore favors

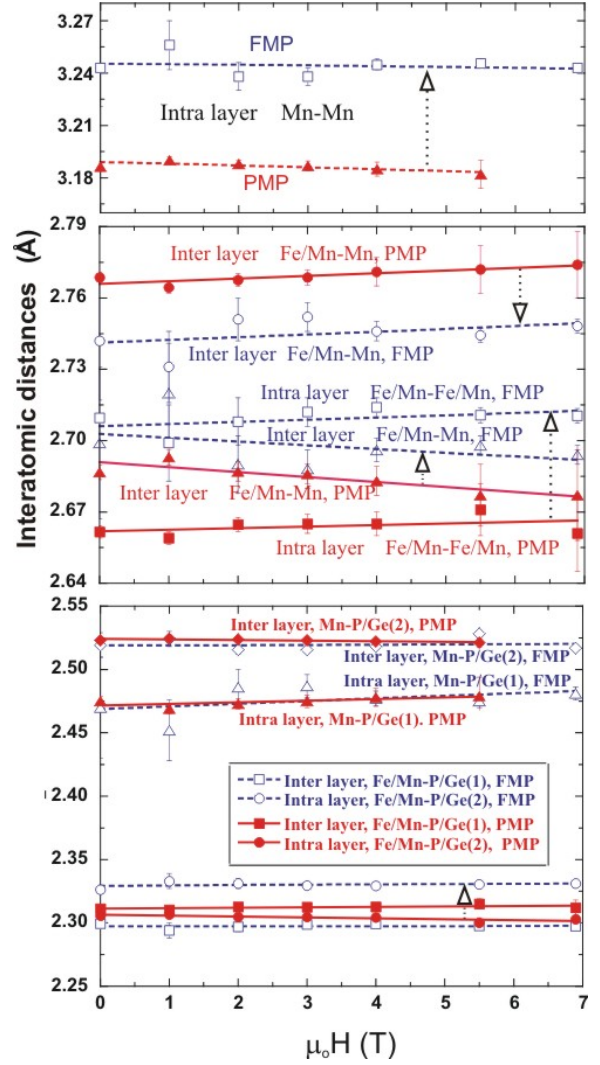


Fig. 8. (color online) Bond distances at 255 K as a function of applied magnetic field. The intra-layer metal-metal distances show sharp increases in going from the PMP to the FMP, while the inter-layer distances decrease (these variations are indicated by the arrows in the figure). The bond distances of the metal—P/Ge do not show a significant variation with field.

the formation of the FMP. Note, however, that the transformation to the FM state is not complete even at 7.0 T, with about 20% of the sample remaining in the PMP. We believe this originates from the non-uniformity of the sample, as discussed previously.¹² The cell

volume of the PMP decreases as the field increases while that of the FMP slightly increases. The lattice parameters also change as the applied field changes (Fig. 7a and 7b). This behavior is consistent with that illustrated in Fig. 3, and can be explained if we assume that different crystallites in the sample have slightly different compositions, and therefore they will convert from one phase to the other at slightly different temperatures, pressure, or field strengths. We have found from the refinement results that at two different values of the applied field (or temperature), the average compositions of the PMP and FMP are different, and therefore the average lattice parameters will be different in the two cases. In other words, the behavior of the parameters indicated in Figs 9a, b, d is further evidence of the existence of inhomogeneities in different parts of the sample. The ordered moments of the Fe and Mn atoms, however, should not change with composition once the transition has taken place, and Fig. 7c shows that this is indeed the case.

The variation of the bond distances as a function of the applied field is illustrated in Fig. 8. One important aspect to note is that all the distances remain remarkably constant when the field varies, indicating that the crystal and magnetic structures of the PMP and FMP do not change markedly as the transformation progresses, as one would expect in a first-order transition. In going from the PMP to the FMP, the variation of the metal-metal distances is positive and large for the intra-layer bonds, and rather small and negative in the case of the inter-layer bonds. The changes of the intra-layer Metal—P/Ge bonds are negligible. This behavior is in general agreement with the behavior shown in Fig. 4, re-enforcing the idea that the effect of temperature on the nature of the transition is basically equivalent to that of an applied magnetic field.

IV. DISCUSSION

The first-order nature of the PM-FM phase transition means that the two phases cannot be expected to coexist over a range of temperatures. However, the large observed range from ≈ 200 K to 255 K is an anomaly whose origin we have attributed to compositional inhomogeneities, which results in a distribution of ordering temperatures.¹² This interpretation is consistent with the fact that, as noted before, the structure has sites with mixed occupancies in which the ratio of the different atomic species can vary significantly with the preparation conditions of the sample. In addition, it is also corroborated by data reported in the literature. For example, Ou *et al.*¹⁵ found large variations of T_c as a function of Mn and Ge content in $\text{Mn}_{1.1}\text{Fe}_{0.9}\text{P}_{1-x}\text{Ge}_x$ and in $\text{Mn}_{1.2}\text{Fe}_{0.8}\text{P}_{1-x}\text{Ge}_x$ for all values of x in the range $0.1 < x < 0.7$. (Fig. 3 of their paper). Similarly, Brück *et al.* [16] showed the effect of Mn substitution on T_c in $(\text{MnFe})_2(\text{PAs})_1$ for constant As content (Fig. 3 of their paper). Better evidence of the presence of compositional inhomogeneities, in our view, is given by our results reported in Figs 3 and 7, showing that there is a variation of the lattice parameters of the PM and FM phases as a function of temperature or applied magnetic field. In samples of uniform composition, the coexistence of the PM and FM phases would be reduced or completely eliminated, and we would obtain a sharp transition in which the entire sample is transformed all at once. It would be helpful, then, to develop preparation procedures to improve the homogeneity.

In summary, the present study emphasizes the importance of the neutron powder diffraction method for understanding the relevant structural details as they relate to the properties of technological importance. In the present study it has been demonstrated that: (i) the phase transition at 255 K is the

only one observed in the temperature range from 10 K to 300 K; (ii) The value of T_c can be increased by doping elements that have the effect of expanding the a and b lattice parameters of the unit cell and increasing the intra-layer metal-metal bond distances; (iii) the application of pressure opposes the expansion of the lattice, and therefore decreases the value of T_c ; (iv) The application of a magnetic field induces the ordering of the magnetic spins of the Fe and Mn atoms, and thus favors the FM phase and increases T_c ; (v) The sample used in our experiments has compositional inhomogeneities which are responsible for a

distribution of T_c 's. Consequently, improvements in the MCE properties can be anticipated if fabrication procedures can be developed to improve the compositional homogeneity.

ACKNOWLEDGMENTS

The authors would like to thank Dr. Antonio Santoro for many helpful discussions. The work in China was supported by the Key Project of Science & Technology Innovation Engineering, Chinese Ministry of Education (Grant No. 705004).

References

*Corresponding author: jeff.lynn@nist.gov

[1] See, for example, the reviews by K. A. Gschneider, Jr., V. K. Pecharsky, and A. O. Tsokol, Rep. Prog. Phys. **68**, 1479 (2005); E. Brück, J. Phys. D, Appl. Phys. **38**, R381 (2005).
 [2] H. Wada and Y. Tanabe, Appl. Phys. Lett. **79**, 3302 (2001).
 [3] V. K. Pecharsky and K. A. Gschneider, Jr., Phys. Rev. Lett. **78**, 4494 (1997).
 [4] O. Tegus, E. Brueck, K. H. J. Buschow and F. R. de Boer, Nature (London) **415**, 150 (2002).
 [5] O. Tegus, B. Fuquam, W. Dagula, L. Zhang, E. Brueck, P. Z. Si, F. R. de Boer and K. H. J. Buschow, J. Alloys Compd **396**, 6 (2005).
 [6] X. W. Li, O. Tegus, L. Zhang, W. Dagula, E. Brueck, K. H. J. Buschow, and F. R. de Boer, IEEE Trans. Magn. **39**, 3148 (2003).
 [7] E. Brueck, O. Tegus, L. Zhang, X. W. Li, F. R. de Boer and K. H. J. Buschow, J Alloys Compd. **383**, 32 (2004).
 [8] D. T. Cam Thanh, E. Brück, O. Tegus, J. C. P. Klaasse T. J. Gortenmulder and K. H. J. Buschow, J. Appl. Phys. **99**, 08Q107 (2006).

[9] W. Dagula, O. Tegus X. W. Li, L. Song, E. Brück, D. T. Cam Thanh, F. R. de Boer, and K. H. J. Buschow, J. Appl. Phys. **99**, 08Q105 (2006).
 [10] W. Dagula, O. Tegus, B. Fuquan, L. Zhang, P. Z. Si, M. Zhang, W. S. Zhang, E. Brueck, F. R. de Boer and K. H. J. Buschow, IEEE Trans. Magn. **41**, 2778 (2005).
 [11] A. Yan, K. H. Mueller, L. Schultz and O. Gutflleischa, J. Appl. Phys. **99**, 08K903 (2006).
 [12] D. M. Liu, M. Yue, J. X. Zhang, T. M. McQueen, J. W. Lynn, X. L. Wang, Y. Chen, J. Li, R. J. Cava, X. Liu, Z. Altounian and Q. Huang, Phys. Rev. B **79**, 014435 (2009).
 [13] A. C. Larson and R. B. Van Dreele, Los Alamos National Laboratory Report No LAUR086-748, 1990 (unpublished).
 [14] K. Ahilan, J. Balasubramaniam, F. L. Ning, T. Imai, A. S. Sefat, R. Jin, M. A. McGuire, B. C. Sales and D. Mandrus, J. Condens. Matter **20**, 472201 (2008).
 [15] Z. Q. Ou, G. F. Wang, L. Song, O. Tegus, E. Brück, and K. H. J. Buschow, Condens. Matter, **18**, 11577 (2006).
 [16] E. Brück, O. Tegus, X. W. Li, F. R. de Boer and K. H. J. Buschow, Physica B **327**, 431 (2003).

Table 1. Structural parameters of $\text{Mn}_{1.1}\text{Fe}_{0.9}\text{P}_{0.8}\text{Ge}_{0.2}$ at 295 and 10 K. Space group $P\bar{6}2m$. Atomic positions: Mn: $3g(x, 0, 1/2)$; Fe/Mn: $3f(x, 0, 0)$; P/Ge(1): $1b(0, 0, 1/2)$; P/Ge(2): $2c(1/3, 2/3, 0)$.

Atom	Parameters	295 K PMP	10 K FMP
Mn	a (Å)	6.06137(7)	6.17811(9)
	c (Å)	3.46023(5)	3.30669(7)
	V (Å ³)	110.098(3)	109.304(3)
	x	0.5916(3)	0.5956(5)
	B (Å ²)	0.77(2)	0.58(2)
	M (μ _B)		3.0(1)
Fe/Mn	$n(\text{Mn/Fe})$	0.998/0.002(3)	0.988/0.012(4)
	x	0.2527(1)	0.2558(2)
	B (Å ²)	0.77(2)	0.58(2)
	M (μ _B)		1.7(1)
P/Ge(1)	$n(\text{Fe/Mn})$	0.928/0.072(3)	0.922/0.078(4)
	B (Å ²)	0.55(4)	0.54(4)
	$n(\text{P/Ge})$	0.947/0.053(8)	0.93/0.07(1)
P/Ge(2)	B (Å ²)	0.55(4)	0.54(4)
	$n(\text{P/Ge})$	0.726/0.274(4)	0.736/0.264(6)
	R_p (%)	5.25	7.05
	wR_p (%)	6.65	8/75
	χ^2	1.276	1.913

Table 2. Selected interatomic distances (Å) and angles (degree) at 295 K and 10 K.

	295 K	10 K
<i>Intra plane metal to metal</i>		
Mn-Mn	3.180(1)	3.254(2)
Fe/Mn-Fe/Mn	2.653(2)	2.738(2)
<i>Inter plane metal to metal</i>		
Mn- Fe/Mn	2.686(2)	2.672(3)
Mn- Fe/Mn	2.771(1)	2.743(2)
<i>Fe/MnP₄ tetrahedron</i>		
Fe/Mn-P/Ge(2) ×2	2.3109(6)	2.3358(7)
Fe/Mn-P/Ge(1) ×2	2.3039(6)	2.2874(8)
<i>MnP₅ pyramid</i>		
Mn-P/Ge(1)	2.476(2)	2.499(3)
Mn-P/Ge(2) ×4	2.5225(5)	2.5026(7)

Table 3. Structural parameters of $\text{Mn}_{1.1}\text{Fe}_{0.9}\text{P}_{0.8}\text{Ge}_{0.2}$ at 239 K under an applied pressure of 0.69 GPa. Space group $P\bar{6}2m$. Atomic positions: Mn: $3g(x, 0, 1/2)$; $\text{Fe}_{0.928(3)}/\text{Mn}_{0.072(12)}/3f(x, 0, 0)$; $\text{P}_{0.928(12)}/\text{Ge}_{0.072(1)}$: $1b(0, 0, 1/2)$; $\text{P}_{0.736(6)}/\text{Ge}_{0.264(6)(2)}$: $2c(1/3, 2/3, 0)$.

Atom	Parameters	0 GPa		0.69 GPa	
		PMP	FMP	PMP	FMP
		19.8(1)%	80.2(1)	26.5(1)%	
	73.5(1)%				
	a (Å)	6.059(4)	6.1515(4)	6.052(1)	
	6.1455(4)				
	c (Å)	3.47(3)	3.3555(3)	3.445(1)	
	3.3473(3)				
	V (Å ³)	109.6(1)	109.96(2)	109.30(4)	
	109.48(2)				
Mn	x	0.64(1)	0.596(2)	0.599(6)	
	0.603(2)				
	B (Å ²)	0.77(2)	0.77(2)	0.6 (1)	0.6(1)
	M (μ _B)		4.4(3)		4.0(2)
Fe/Mn	x	0.243(5)	0.2550(8)	0.253(3)	
	0.2538(8)				
	B (Å ²)	0.7(1)	0.7(1)	0.6(1)	0.6(1)
	M (μ _B)		1.0(2)		1.0(2)
P/Ge(1)	B (Å ²)	0.5(1)	0.5(1)	0.6(1)	0.4(1)
P/Ge(2)	B (Å ²)	0.5(1)	0.5(1)	0.6(1)	0.4(1)
	R (%)		2.44		2.35
	wR (%)		3.13		2.94
	χ^2		2.433		2.129